

## Self-consistent Al (111) film calculations

Kenneth Mednick and Leonard Kleinman

Department of Physics, University of Texas, Austin, Texas 78712

(Received 27 June 1980)

We have performed self-consistent linear-combination-of-Gaussian-orbitals calculations for six-layer Al (111) films using the Kohn-Sham exchange and two different forms for the correlation potential. Using the Wigner correlation potential, we obtain a work function of 4.275 eV; this is the first Al calculation in agreement with the experimental value of 4.26 eV. Stretching the six-layer potential to 18 layers, we calculate the energy bands and find several surface states, two of which have not appeared in previous calculations.

### I. INTRODUCTION

In our early calculations of the electronic structure of Al films<sup>1</sup> we constructed a film pseudopotential by superposing atomic pseudopotentials and smoothly joining their planar average to the jellium potential<sup>2</sup> outside the film. For the (111) film, because of its lower symmetry, we were able to obtain convergence of our plane-wave expansions of the wave functions only at symmetry points in the two-dimensional Brillouin zone (2DBZ). Chelikowsky *et al.*,<sup>3</sup> performed a self-consistent pseudopotential calculation of Al (111), and although they found agreement with us in the surface-state structure at  $\bar{\Gamma}$ ,  $\bar{K}$ , and  $\bar{M}$ , they found a dip in the planar average of their self-consistent pseudopotential near the film surface. In spite of the fact that this dip induced a Friedel oscillation in the surface charge density similar to that found in jellium with a large  $r_s$  (jellium with the density of aluminum has essentially no Friedel oscillation<sup>2</sup>), they concluded their calculation cast doubt on our procedure of matching jellium to bulk potentials. (We concluded that our procedure was satisfactory and that their calculation was unconverged.) They also concluded that their calculated work function of 5.2 eV was in satisfactory agreement with the experimental value<sup>4</sup> of  $4.26 \pm 0.03$  eV. Very recently Wang *et al.*<sup>5</sup> performed a self-consistent, warped-muffin-tin potential, linearized augmented-plane-wave Al (111) calculation and obtained a work function of 4.7 eV.

In this paper we present the results of very accurate self-consistent linear-combination-of-Gaussian-orbitals (LCGO) calculation for six-layer Al (111) films using the Kohn-Sham<sup>6</sup> exchange potential and both the von Barth-Hedin<sup>7</sup> and Wigner<sup>8</sup> correlation potentials (in Ry atomic units)

$$V_{\text{vBH}} = -0.0504 \ln(1 + 30/r_s), \quad (1)$$

$$V_{\text{W}} = -0.88 \left( \frac{4}{3} r_s + 7.79 \right) / (r_s + 7.79)^2, \quad (2)$$

in order to test their effect on the work function. Using  $V_{\text{W}}$  we obtain a work function of 4.275 eV in perfect agreement with experiment. We also stretch the film to 18 layers and calculate the energy bands throughout the 2DBZ, finding several surface states, two of which have not been found in earlier calculations. In the next section we describe our LCGO procedure and in the third section our results are presented.

### II. COMPUTATIONAL TECHNIQUE

The LCGO scheme requires that the charge density at each iteration be expanded in Gaussians and plane waves. We use two short-range Gaussians on each atomic site of the form

$$(A_1 \beta_1 / \pi) (\beta_1 r^2 - 0.5) e^{-\beta_1 r^2} / r \\ + (A_2 \beta_2 / \pi) (\beta_2 r^2 - 0.5) e^{-\beta_2 r^2} / r,$$

with the conditions  $A_1 + A_2 = Z$  and  $A_1 \beta_1 + A_2 \beta_2 = 0$ . The former ensures that the electronic charge associated with each site cancels the nuclear charge  $Z$  and together with the nuclear charge yields a Coulomb potential  $V(r) = -(A_1 e^{-\beta_1 r^2} + A_2 e^{-\beta_2 r^2}) / r$ . The latter condition is required to keep the electronic charge finite at the nucleus. At each atomic site we have 30 Gaussians of the form  $(\beta/\pi)(1.5 - \beta r^2)e^{-\beta r^2}$  which contain no net charge and yield Coulomb potentials  $e^{-\beta r^2}$ . The values of  $\beta$  chosen ranged between 0.1 and 20 000 bohrs<sup>-2</sup>. Rather than use nonspherical Gaussians as we did in bulk calculations,<sup>9</sup> we supplemented the 96 spherical Gaussians with 228 plane-wave Gaussians in the half-film of the form

$$\pi^{-1} \left[ \frac{1}{4} \bar{G}^2 + \frac{1}{2} \beta - \beta^2 (z - z_0)^2 \right] e^{-\beta (z - z_0)^2} e^{i \bar{G} \cdot \bar{r}}$$

(which yield Coulomb potentials of the form  $e^{-\beta (z - z_0)^2} e^{i \bar{G} \cdot \bar{r}}$ ) for the eight lowest symmetrized combinations of two-dimensional reciprocal-lattice vectors (including  $\bar{G} = 0$ ). In units of interplanar spacings with atomic planes at 0.5, 1.5, and 2.5, the  $z_0$  went from 0.125 to 3.875 in steps

of 0.25 with additional  $\bar{G}=0$  Gaussians interleaved from  $z_0=2.25$  to 4. The values used for  $\beta$  depended upon whether we used one or two  $\beta$ 's for a particular  $z_0$  and  $\bar{G}$  and on the  $z_0$  spacing. For instance, for  $\bar{G}=0$  and  $z_0 \geq 2.25$  we used  $\beta=3$  and 10, but for  $z_0 \leq 2.125$  we used only  $\beta=1.5$ .

We calculated the charge at 2733 points in the  $\frac{1}{8}$ th irreducible wedge of the unit cell of the half-film; of these, 82 were chosen on a radial mesh, alternating between the forward [111] and backward  $[\bar{1}\bar{1}\bar{1}]$  directions within each of the three atomic cores in the half-film unit cell. The remaining 2487 points were chosen randomly throughout the wedge.<sup>10</sup> We calculated the energy bands at 73 points in the  $\frac{1}{12}$ th irreducible 2DBZ to determine the Fermi surface and then used a 19-point subset in a triangle integration scheme<sup>11</sup> to obtain the charge density at the 2733 points. Other workers have used as small a 2DBZ sample as 3 points.<sup>12</sup> The charge was fitted by varying the coefficients of the Gaussians to minimize a weighted rms error at the 2733 points. The magnitude of the rms error, though less than that in our bulk calculations,<sup>9</sup> is not a significant quantity since it increases with the number of points fit and depends on the weighting. The error in the fit was sufficiently small that we were able to converge the eigenvalues to a largest deviation of 0.005 eV in any core eigenvalue between successive iterations (valence deviations were several times smaller). At that point random errors, probably in the fit, caused further iteration to be useless. Because we chose our charge Gaussians to be  $-\nabla^2 V(r)/4\pi$ , where  $V(r)$  stands for one of our various Coulomb Gaussians, fitting the charge density automatically fit the Coulomb potential. The exchange and correlation potentials were calculated from the charge density at the 2733 points and fitted with the 90  $e^{-\beta r^2}$  and 228 plane wave  $e^{-\beta(z-z_0)^2} e^{i\bar{G}\cdot\vec{r}}$  Gaussians.

It is worthwhile to compare our fitting procedure with that used by other workers. Feibelman *et al.*<sup>13</sup> fitted with spherical Gaussians only, but by including many floating sites as well as atomic sites achieved an accuracy presumably comparable to ours. They, however, used  $e^{-\beta r^2}$  rather than  $\nabla^2 e^{-\beta r^2}$ -type Gaussians to fit the charge, necessitating a separate fit of the Coulomb potential. Wang and Freeman<sup>14</sup> fit the Ni (001) charge density with spherical atomic charges,  $3d^4 4s^1 4p^6$ , with only three parameters ( $x$ ,  $y$ , and  $z$ ) per atomic site. We found in the one case where we tested it that a 30% greater rms error was obtained when we dropped the plane-wave Gaussians and fitted with 32 spherical Gaussians (30 free parameters) per lattice site only. Furthermore, the planar average of the charge in the surface

region was noticeably different, which is expected to have a large effect on the work function.<sup>15</sup> Smith *et al.*<sup>16</sup> calculate the difference between a superposition of atomic charges and the calculated charge at 763 points in an irreducible wedge of a 9-layer Cu unit cell. They find typically a 2% discrepancy in the total charge which they remove with a multiplicative factor. When we remove our charge-conserving subsidiary condition to test our fit, we typically find a 0.05% error in the conduction-band charge. Furthermore, their 763 points are on a regular mesh so that when they Fourier-transform their charge-density difference, they do not see small but significant changes in the core region which occur because the atomic configuration which best fits the film charge density is not their starting (atomic ground-state) configuration. We believe that a combination of these procedures, i.e., fitting the atomic charge configuration as Wang and Freeman do and then Fourier-transforming the difference between that charge density and the calculated charge density, might give a very good fit.

Our original basis set consisted of 1s, 2s, 2p, 3s, and 3p atomic orbitals which were expanded in 13 Gaussians ( $e^{-\alpha r^2}$  with  $\alpha$  ranging between 0.080 and 9000 bohrs<sup>-2</sup>) plus s and p Gaussians with  $\alpha=0.080$  on each atomic site. We supplemented this with  $\alpha=0.130$  s and p Gaussians on the surface-plane atomic sites plus  $\alpha=0.300$  s and p Gaussians on B and C sites (assuming the surface-plane atomic sites are A sites), 0.3 interplanar spacings above the surface plane. This gives a total of 102 basis functions for the six-layer films and 258 for the 18-layer. After adding the additional surface Gaussians, the work function dropped 0.3 eV, indicating the importance of having sufficient variational freedom in the surface region. Among the various LCGO calculations only those of Feibelman *et al.*<sup>13</sup> appear to

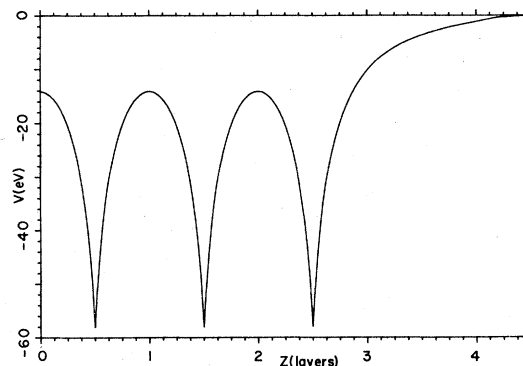


FIG. 1. Planar average of the total self-consistent potential in half of a six-layer Al (111) film with the Wigner correlation potential. The abscissa is in units of interplanar spacings.

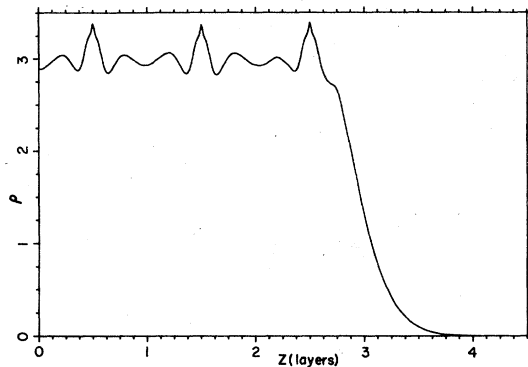


FIG. 2. Planar average of the valence charge density of half of a six-layer Al (111) film with the Wigner correlation potential in units of electrons per atom. The abscissa is in units of interplanar spacings.

have this much variational freedom.

We stretched the six-layer film to 18 layers by first fitting the potential in the central half-layer of the six-layer film with an array of spherical and quartic Kubic harmonic Gaussians with full cubic symmetry. We assume this bulk potential exists over the twelve central layers of the film. We fit the 18-layer film by first fixing the spheri-

cal and quartic Gaussians with their bulk coefficients on the twelve central layers. This of course exactly fits the assumed potential in the interior of the twelve bulk layers, but not near their interface with the surface layers. We then fit the difference between the 18-layer potential and the contribution of the twelve central layers of Gaussians over the region between 4.75 and 10 interplanar spacings (where the center of the film is at 0, the bulk layers run from  $\pm 0.5$  to  $\pm 5.5$  and the surface layers from  $\pm 6.5$  to  $\pm 8.5$ ) using the same Coulomb Gaussians that we used for the six-layer film, but supplemented with additional plane-wave Gaussians in the interface region. Although the planar average of the potential in the four central layers of the six-layer film appears bulklike (see Fig. 1), the potential itself is not, and even in the central layer does not have cubic symmetry. Thus when we fitted the central layer potential using Gaussians with full cubic symmetry, we introduced an error which showed up as an oscillating discrepancy of magnitude 0.02 eV between the planar average of the potential in the interior of the 6- and 18-layer films. In spite of this we believe our stretching procedure should be somewhat more accurate than that used by Feibelman

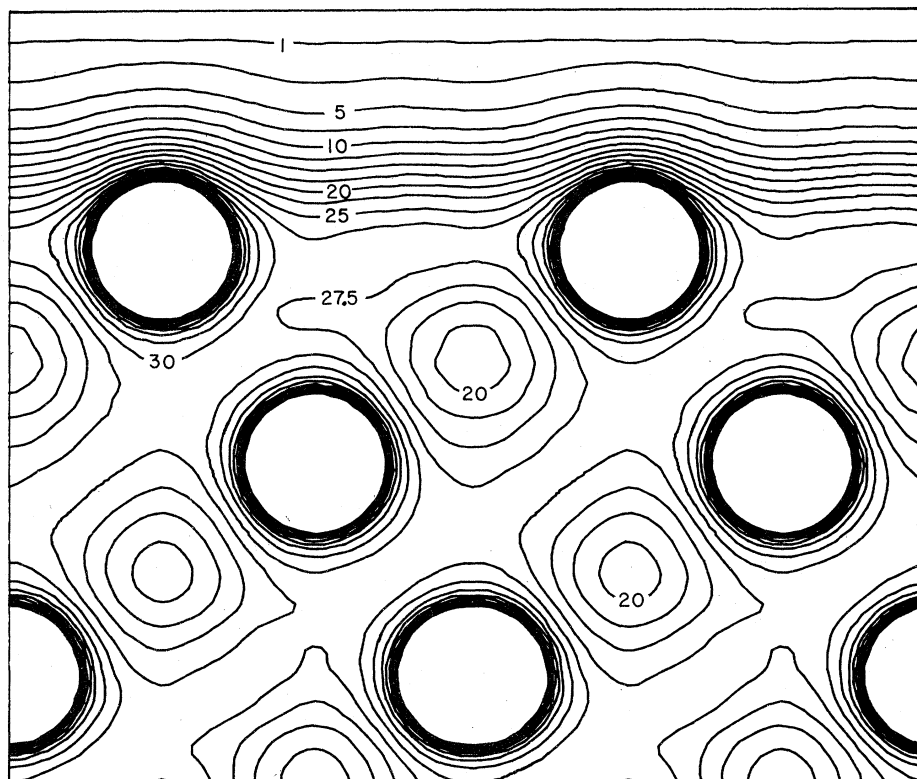


FIG. 3. Contour plot of the total charge density of a six-layer Al (111) film with the Wigner correlation potential in the  $(\bar{1}10)$  plane in units of millielectrons per cubic bohr. Except for the unit contour, all contours are 2.5 times an integer.

*et al.*,<sup>13</sup> who used bulk Hamiltonian matrix elements between pairs of basis functions whenever one of the basis functions was centered in the interior region, even if the other was not. In any event, our method could be improved by iterating on the bulk potential until it was self-consistent, but we did not feel that was worthwhile.

### III. ENERGY BANDS OF Al (111)

Because the extended x-ray absorption fine structure (EXAFS) (Ref. 17) and one low-energy electron diffraction (LEED) calculation<sup>18</sup> show a small contraction while all other LEED calculations<sup>19,20</sup> show a small dilation of the (111) surface of Al, we chose the bulk interplanar spacing for all layers in our films. In Fig. 1 we show the planar average of the self-consistent potential for a six-layer film with the Wigner correlation potential, and in Fig. 2 the planar average of the valence charge density of the same film. Note that unlike Chelikowski *et al.*,<sup>3</sup> we find no dip in the potential near the surface and no Friedel oscillation in the surface charge density, in agreement with the results for jellium of this density.<sup>2</sup> A contour plot of the total charge density in the  $(\bar{1}10)$  plane is shown in Fig. 3. The calculated work function for this film is 4.275 eV in perfect agreement with the experimental value<sup>4</sup> of  $4.26 \pm 0.03$  eV.

In order to test the dependence of the work function on the choice of correlation potential, we repeated the calculation using the vBH potential.<sup>7</sup> The calculated work function is 4.545 eV. If one substitutes  $r_s = 2.07$  in Eqs. (1) and (2), one finds the jellium average of  $V_{\text{vBH}}$  is 0.58 eV below that of  $V_w$ . In Fig. 4 we plot the difference between the Wigner and vBH planar averages of potential and charge density. The vBH potential averages about 0.24 eV below the Wigner in the interior of the

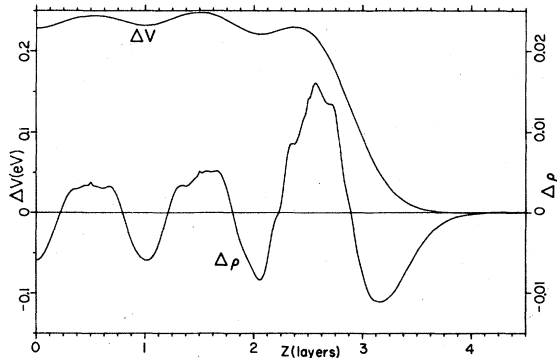


FIG. 4. Differences between planar averages of potential and valence charge density for six-layer Al (111) films with Wigner and vBH correlation potentials in same units as Figs. 1 and 2.

film, i.e., about 0.34 eV of the extra vBH correlation potential is screened out by the surface double layer seen in the charge difference plot.

In Fig. 5 we plot the energy bands of the Wigner film stretched to 18 layers as described in the preceding section. We show the projection of the bulk bands at the symmetry points.<sup>21</sup> The symmetries below the vacuum level are only  $\bar{\Gamma}_1^+$ ,  $\bar{M}_1^+$ , and  $\bar{K}_1^+$  and  $\bar{K}_2^+$ ; because  $\bar{K}$  is projected from a line of no symmetry in the 3DBZ,  $\bar{K}_1$  and  $\bar{K}_2$  have the same projection. Along the symmetry lines, at  $\bar{\Sigma}$  only  $\bar{\Sigma}_1$  states occur below the vacuum, at  $\bar{T}$  ( $\bar{T}'$ ) both  $\bar{T}_1$  and  $\bar{T}_2$  ( $\bar{T}'_1$  and  $\bar{T}'_2$ ) occur, but since they span the same bulk continuum, they are not distinguished in the figure. The conduction-band width (from the lowest  $\bar{T}_1$  to  $E_F$ ) is 0.82 Ry (0.80 Ry) in the six-layer Wigner (vBH) film, and if one assumes  $E_F$  unchanged, it is 0.83 Ry in the 18-layer film. This is to be compared with the bulk value<sup>22</sup> of 0.815 Ry (Kohn-Sham exchange, no correlation potential) and the jellium value of 0.86 Ry. The reduction from the jellium value is due to the fact that  $k=0$  electrons have a greater overlap with the core than  $k=k_F$  electrons and hence "see" a stronger repulsive orthogonalization potential.

To find the surface states at the symmetry points, we plotted all the wave functions  $\psi(\vec{r}, r_1)$  as a function of  $r_1$  for fixed  $\vec{r}$ . We chose  $\vec{r}$

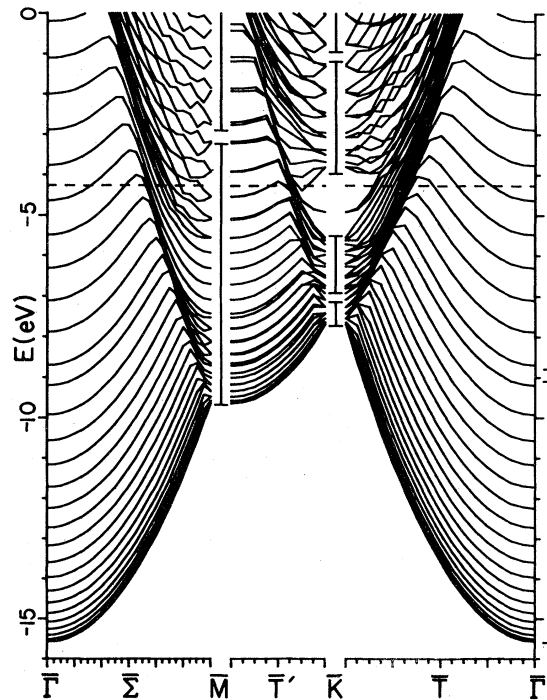


FIG. 5. Energy bands of 18-layer Al (111) film with Wigner correlation potential. The bulk bands are projected at  $\bar{\Gamma}$ ,  $\bar{M}$ , and  $\bar{K}$ . The dashed line is the Fermi energy.

$=a(\frac{1}{6}, -\frac{1}{6}, 0)$  which is equally far from the atomic sites in  $A$ ,  $B$ , and  $C$  planes. When we took  $\bar{r} = (000)$  which passes through atoms on  $A$  planes, the large core oscillations of the valence functions (which generally were not symmetric) quite often obscured the nature of the function. Taking the  $(2\pi/a)(-\frac{1}{3}, -\frac{1}{3}, \frac{2}{3})$   $\bar{M}$  point and the  $(2\pi/a)(\frac{2}{3}, -\frac{2}{3}, 0)$   $\bar{K}$  point,  $\bar{r}$  is a two-fold axis in the group of the wave vectors of  $\bar{\Gamma}$ ,  $\bar{M}$ , and  $\bar{K}$ , thus making our wave-function plots either even or odd under reflection through the central plane of the film. In Fig. 6 we show the  $\bar{M}_1^+$  and  $\bar{M}_1^-$  surface-state wave functions at  $-3.170$  and  $-3.216$  eV which lie in the bottom of the gap in the  $\bar{M}$  projection. These have a very long decay length and decay irregularly so that the skeptical reader may not be convinced by our 18-layer film plot that in a thicker film these will form a degenerate pair of surface states.

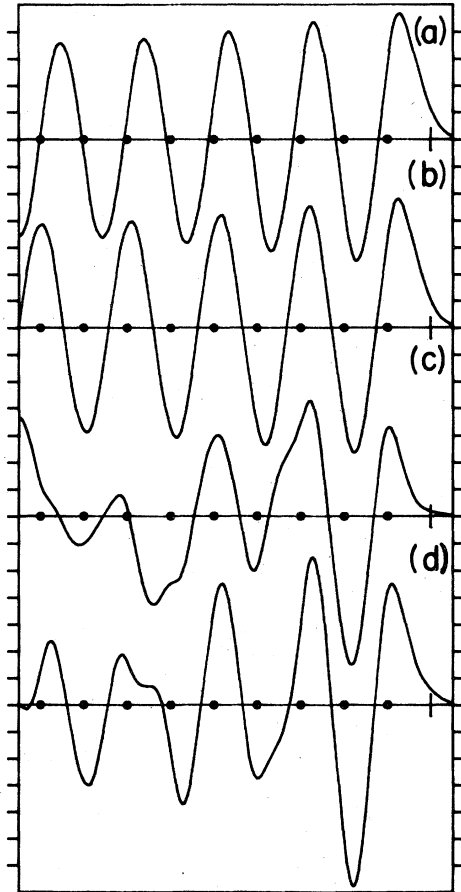


FIG. 6. Plots of  $\bar{M}$  and  $\bar{\Gamma}$  surface-state wave functions  $\psi(\bar{r}, r_1)$  for  $r = a(\frac{1}{6}, -\frac{1}{6}, 0)$  in half of an 18-layer Al (111) film. The dots represent planes of atoms and the ticks mark the first missing plane outside the film. (a)  $\bar{\Gamma}_1^+$  at  $-8.703$  eV; (b)  $\bar{\Gamma}_1^-$  at  $-9.206$  eV; (c)  $\bar{M}_1^+$  at  $-3.170$  eV (d)  $\bar{M}_1^-$  at  $-3.216$  eV. The units are arbitrary but  $\bar{M}_1^+$  is drawn to twice the scale of  $\bar{\Gamma}_1^+$ .

The  $\bar{\Gamma}_1^+$  and  $\bar{\Gamma}_1^-$  surface-state wave functions at  $-8.703$  and  $-9.206$  eV shown in the same figure have an even longer decay length and a much larger splitting of their thick film degeneracy. This splitting is so large that these states lie above and below the gap in the  $\bar{\Gamma}$  projection of the bulk bands. However, because of the smoothness in their decay, their surface-state nature is convincingly shown in Fig. 6. This smoothness follows from the fact that the  $\bar{\Gamma}_1^+$  surface states come mainly from  $\bar{k} = (2\pi/a)(\frac{1}{2}, \frac{1}{2}, \frac{1}{2})$  in the 3DBZ so that  $k_1 r_1$  changes by  $\pi$  over an interplanar spacing coupled with our choice of  $\bar{r}$  which makes  $A$ ,  $B$ , and  $C$  planes equivalent. Because of this smoothness, the surface-state nature of these wave functions

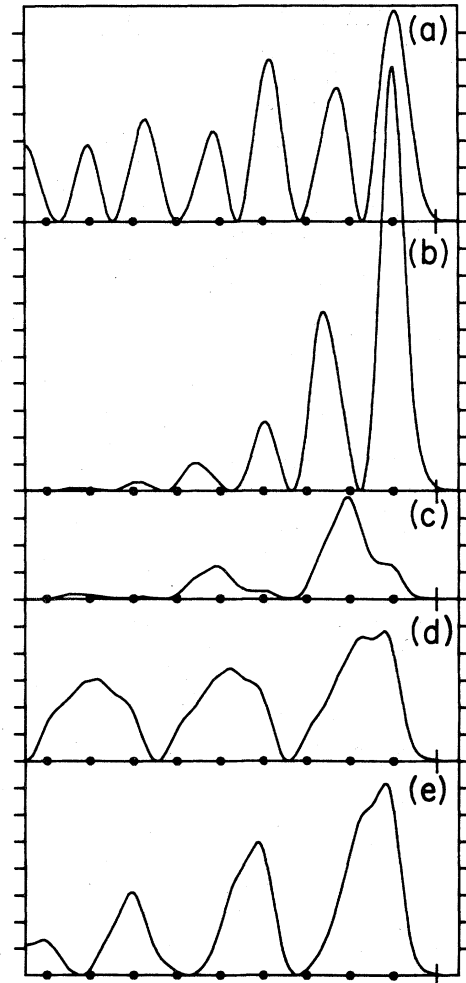


FIG. 7. Plots of  $\bar{K}_1^+$ ,  $\bar{K}_1^-$ , and even partner of  $\bar{K}_2$  surface-state charge densities  $|\psi(\bar{r}, r_1)|^2$  for  $\bar{r} = a(\frac{1}{6}, -\frac{1}{6}, 0)$  in half of an 18-layer Al (111) film. The dots represent planes of atoms and the ticks mark the first missing plane outside the film. (a)  $\bar{K}_2$  at  $-3.813$  eV; (b)  $\bar{K}_1^-$  at  $-4.920$  eV; (c)  $\bar{K}_2$  at  $-7.085$  eV; (d)  $\bar{K}_1^+$  at  $-6.802$  eV; (e)  $\bar{K}_1^-$  at  $-6.919$  eV.

also shows up in a Mulliken analysis, and we are able to see the surface-state nature of these bands more than half-way to  $\bar{M}$  and  $\bar{K}$  along  $\bar{\Sigma}$  and  $\bar{T}$ .

For the  $\bar{\tau}$  chosen here the wave functions at  $\bar{K}$  are complex; rather than show the real and imaginary parts separately, in Fig. 7 we plot  $|\psi(\bar{\tau}, r_1)|^2$  for the  $\bar{K}_1^+$ ,  $\bar{K}_1^-$ , and the even partner<sup>23</sup> of the degenerate  $\bar{K}_2$  surface states. We could find no surface states in or near the projected gap at  $-1.1$  eV. Previously<sup>1(c)</sup> in a non-self-consistent 33-layer film we were barely able to distinguish a surface state in this gap. Whether or not a surface state with an extremely long decay length exists in this gap in thick films we, of course, cannot say. In the big gap around the Fermi energy we find a well-localized  $\bar{K}_2$  surface state at  $-4.920$  eV which extends more than  $\frac{1}{8}$ th the way to  $\bar{M}$  along  $\bar{T}'$  and more than  $\frac{1}{16}$ th the way to  $\bar{\Gamma}$  along  $\bar{T}$ . In addition, just above the gap at  $-3.813$  eV is another  $\bar{K}_2$

surface state which has not been found in previous calculations. In a very thick film this surface state would lie just at the top of the gap and a slight change in surface potential could force it into the continuum. In the lowest  $\bar{K}$  gap we find a fairly well localized  $\bar{K}_2$  surface state at  $-7.085$  eV; at the top of the gap we find a  $\bar{K}_1^-$  surface state at  $-6.919$  eV and its thick film degenerate  $\bar{K}_1^+$  partner lies slightly above the gap at  $-6.802$  eV. We previously found<sup>1(c)</sup> this  $\bar{K}_1^+$  pair, and Chelikowski *et al.*<sup>3</sup> found a pair whose symmetry they did not give, but this is the first calculation in which two pairs of surface states have been associated with this gap.

#### ACKNOWLEDGMENT

This work was supported by the National Science Foundation under Grant No. DMR 77-21559.

<sup>1</sup>E. B. Caruthers, L. Kleinman, and G. P. Alldredge, (a) Phys. Rev. B **8**, 4570 (1973); (b) **9**, 3325 (1974); (c) **9**, 3330 (1974).

<sup>2</sup>N. D. Lang and W. Kohn, Phys. Rev. B **1**, 4555 (1970).

<sup>3</sup>J. R. Chelikowsky, M. Schlüter, S. G. Louie, and M. L. Cohen, Solid State Commun. **17**, 1103 (1975).

<sup>4</sup>R. M. Eastment and C. H. B. Mee, J. Phys. F **3**, 1738 (1973).

<sup>5</sup>D. S. Wang, A. J. Freeman, H. Krakauer, and M. Posternak, Bull. Am. Phys. Soc. **25**, 193 (1980).

<sup>6</sup>W. Kohn and L. J. Sham, Phys. Rev. **140A**, 1133 (1965).

<sup>7</sup>U. von Barth and L. Hedin, J. Phys. C **5**, 1629 (1972).

<sup>8</sup>G. P. Alldredge and L. Kleinman, Phys. Rev. B **10**, 559 (1974).

<sup>9</sup>L. Kleinman and K. Mednick, Phys. Rev. B **20**, 2487 (1979); **21**, 1549 (1980).

<sup>10</sup>If a regular array of points were chosen, the plane-wave Gaussians would fit the charge extremely well on each plane of points, but give large unphysical excursions in the charge between planes.

<sup>11</sup>C. S. Wang and A. J. Freeman, Phys. Rev. B **19**, 793 (1979), Appendix A.

<sup>12</sup>F. J. Arlinghaus, J. G. Gay, and J. R. Smith, Phys. Rev. B **21**, 2055 (1980).

<sup>13</sup>P. J. Feibelman, J. A. Appelbaum, and D. R. Hamann, Phys. Rev. B **20**, 1433 (1979).

<sup>14</sup>C. S. Wang and A. J. Freeman, Phys. Rev. B **19**, 793 (1979).

<sup>15</sup>A fit of the potential with spherical Gaussians on lattice sites only was extremely poor because of the long exchange-potential tail extending outside the film.

<sup>16</sup>J. R. Smith, J. G. Gay, and F. J. Arlinghaus, Phys. Rev. B **21**, 2201 (1980).

<sup>17</sup>A. Bianconi and R. Z. Bachrach, Phys. Rev. Lett. **42**, 104 (1979).

<sup>18</sup>D. L. Adams and U. Landman, Phys. Rev. B **15**, 3775 (1977).

<sup>19</sup>H. L. Yu, M. C. Muñoz, and F. Soria, Surf. Sci. **94**, L184 (1980).

<sup>20</sup>D. W. Jepsen, P. M. Marcus, and F. Jona, Phys. Rev. B **8**, 1786 (1973).

<sup>21</sup>A projection of the entire 2DBZ in qualitative agreement with this projection of the symmetry points is shown in Fig. 3 of Ref. 1(c).

<sup>22</sup>S. P. Singhal and J. Callaway, Phys. Rev. B **16**, 1744 (1977).

<sup>23</sup>By even we mean even under  $r_1 \rightarrow -r_1$  for  $\bar{\tau} = a(\frac{1}{6}, -\frac{1}{6}, 0)$ .